Received: 30 January 2022 | Revised: 11 April 2022

DOI: 10.1002/JLB.3HI0422-635R

JLB JOURNAL OF LEUKOCYTE BIOLOGY

HIGHLIGHTED ARTICLE

Antiretroviral therapy restores the homeostatic state of microglia in SIV-infected rhesus macaques

Andrew J. Trease[1] | Meng Niu[2] | Brenda Morsey[1] | Chittibabu Guda[2] | Siddappa N. Byrareddy[3] | Shilpa Buch[3] | Howard S. Fox[1]

[1]Department of Neurological Sciences, University of Nebraska Medical Center, Omaha, Nebraska, USA

[2]Department of Genetics, Cell Biology and Anatomy, University of Nebraska Medical Center, Omaha, Nebraska, USA

[3]Department of Pharmacology and Experimental Neuroscience, University of Nebraska Medical Center, Omaha, Nebraska, USA

Correspondence
Howard Fox, Department of Neurological Sciences, University of Nebraska Medical Center, Omaha, NE 68198, USA.
Email: hfox@unmc.edu

Abstract

Microglia and macrophages are essential for homeostatic maintenance and innate immune response in the brain. They are the first line of defense against infections such as HIV/SIV in the brain. However, they are susceptible to infection and function as viral reservoirs even under effective viral suppression. While current antiretroviral regimens successfully suppress viremia and improve quality of life and lifespan, neurologic complications persist and are in part attributed to activated microglia. We sought to test the hypothesis that brain microglia return to a more homeostatic-like state when viremia is suppressed by combination antiretroviral therapy. Using the SIV-rhesus macaque model, we combined single-cell RNA sequencing, bioinformatics, and pathway analysis to compare gene expression profiles of brain myeloid cells under 4 conditions: uninfected, SIV infected, SIV infected with cART suppression, and SIV encephalitis (SIVE). Our study reveals greater myeloid diversity and an elevated proinflammatory state are associated with untreated SIV infection compared with uninfected animals. The development of encephalitis and suppression of viremia both reduced myeloid diversity. However, they had converse effects on the activation state of microglia and inflammation. Notably, suggestive of a restoration of a homeostatic state in microglia, gene expression and activation of pathways related to inflammation and immune response in cART-suppressed monkeys were most similar to that in uninfected monkeys. Untreated SIV infection shared characteristics, especially in brain macrophages to SIVE, with SIVE showing dramatic inflammation. In support of our hypothesis, our study demonstrates that cART indeed restores this key component of the brain's homeostatic state.

Summary: ScRNA-seq of rhesus monkey microglia reveals clusters of cells in activated states in the setting of SIV infection, which is primarily reversed by suppressing viremia with combination antiretroviral therapy.

Abbreviations: AIF1, allograft inflammatory factor 1; APOBEC3A, apolipoprotein B mRNA editing enzyme catalytic subunit 3A; APOC1, apolipoprotein C1; ART, antiretroviral therapy; CAM, CNS-associated macrophages; cART, combination antiretroviral therapy; CPM, counts per million reads; CSF1R, colony-stimulating factor 1 receptor; DEG, differentially expressed gene; F13A1, coagulation factor XIII A chain; FCN1, ficolin 1; IFI27, IFN alpha inducible protein 27; IFNB1, IFN beta 1; IL1RN, IL-1 receptor antagonist; IPA, ingenuity pathway analysis; IRF, IFN response factor; ISG15, IFN-stimulated gene 15; MEF2C, myocyte-specific enhancer factor 2C; NHP, nonhuman primate; PCA, principal component analysis; PWH, people (persons) with HIV; qRT-PCR, quantitative reverse transcription-PCR; scRNA-seq, single-cell RNA-sequencing; SIVE, SIV encephalitis; SPI1, Spi-1 proto-oncogene (also known as PU.1); SPP1, secreted phosphoprotein 1 (also known as osteopontin); SRV, simian type D retrovirus; STLV-1, simian T-lymphotropic virus 1; UMAP, uniform manifold approximation and projection; UMI, unique molecular identifier; UNMC, University of Nebraska Medical Center.

KEYWORDS
brain, HIV, macrophage, neuroHIV, scRNA-seq

1 | INTRODUCTION

SIV and HIV are primate lentiviruses with a high degree of genomic, structural, and virologic similarity. In vivo, both viruses cause persistent infection. Infection of nonhuman primates (NHPs) by SIV mimics many central aspects of HIV infection in humans, including immune deficiency, opportunistic infections, and CNS disease.[1–9] The amenability of this model to antiretroviral therapy (ART) creates a valuable system in which to mimic the conditions found in people with HIV (PWH), including the effects of chronic infection and the persistence of viral reservoirs. NHP infection by SIV remains the best model to date for the study of HIV pathogenesis and treatment, including neuropathogenesis.[10–14]

In monkeys, as in people, the viral targets include not only CD4+ T cells but also brain macrophages and microglia.[15,16] While studies on the brain prior to the current era of treatment largely focused on dementia and encephalitis, both the clinical and neuropathologic pictures have changed following the introduction of combination ART (cART), where both the neurocognitive and neuropathologic findings are less profound, and the relationship to the prior pathogenic mechanisms unclear.[17–20] Our understanding of CNS HIV infection and its effects have evolved along with the transition of HIV from a lethal infection to a treatable condition, however much is still unknown. Regardless of treatment, several aspects remain unaltered: productive HIV infection in the brain is limited to macrophages and microglia, and neuronal dysfunction is indirect due to alterations in the infected cells that can affect neurons.[21,22] Such a process leads to a condition referred to by various terms depending on the pandemic era and diagnostic criteria, such as HIV-associated dementia, minor cognitive-motor disorder, asymptomatic neurocognitive impairment, and mild neurocognitive disorder.[23,24] These is known collectively as the HIV-associated neurocognitive disorder;[24] an alternate term now used by some is neuroHIV.

The brain has a variety of cell types. There are dozens of different neurons, the key cells that carryout vital functions. In addition, there are many nonneuronal cell types in the brain, including the cells known collectively as glia: astrocytes, oligodendrocytes, and microglia. Furthermore, there are various progenitor cells, support cells such as endothelial cells and pericytes, and CNS-associated macrophages (CAM, also known as border-associated macrophages). Both microglia and macrophages are part of the myeloid innate immune system. Although microglia are placed in the glia category, and macrophages can arise from blood-borne monocytes, both microglia and CAM have a distinct origin from the extraembryonic yolk sac early in development.[25,26] These cells respond to virus infection by exhibiting an inflammatory state. Thus, they likely drive HIV neuropathogenesis, where even in the current cART era, a low level of ongoing HIV-1 viral replication and/or production of early viral protein(s) by activated microglia likely promotes the symptomatology of neuroHIV, as well as serve as a reservoir for the virus during cART suppression.[16]

A focus on brain microglia and macrophages in different stages of HIV infection is key to determining the effect of HIV on the brain. We have long studied the immune cells, predominantly microglia, from the brains of SIV-infected rhesus monkeys under various conditions. In addition to studying fresh cells, we cryopreserve cells and have shown that these represent a good source of material for a variety of studies, including single-cell RNA-sequencing (scRNA-seq).[27,28] To assess these key cells in the brain under a variety of relevant conditions, here we used scRNA-seq to examine the transcriptome of brain myeloid cells (microglia and macrophages) from 4 groups of monkeys: uninfected, SIV infected without treatment (SIV untreated), SIV infected with cART-treatment (SIV treated), as well as those with SIV encephalitis (SIVE).

2 | METHODS

2.1 | Experimental model and subject and macrophage/microglia preparation details

Twelve males, 3–7-years-old rhesus macaques were purchased from Alpha-Genesis Primate Research Center (Yemassee, SC), PrimGen (Hines, IL), or New Iberia Research Center (New Iberia, LA). The monkeys tested negative for the indicated viral pathogens: SIV, SRV, STLV-1, Herpes B-virus, and measles; and bacterial pathogens: salmonella, shigella, campylobacter, yersinia, and vibrio. Macaques were housed in compliance with the Animal Welfare Act and the Guide for the Care and Use of Laboratory Animals in the NHP facilities of the Department of Comparative Medicine, University of Nebraska Medical Center (UNMC). The primate facility at UNMC has been accredited by the American Association for Accreditation of Laboratory Animal Care international. The UNMC Institutional Animal Care and Use Committee reviewed and approved this study under protocols 08-035-07-FC, 11-032-05-FC, and 16-073-FC. Animals were maintained in a temperature-controlled (23 ± 2°C) indoor climate with a 12-h light/dark cycle. They were fed Teklad Global 25% protein primate diet (#2055; Envigo, Madison, WI) supplemented with fresh fruit or vegetables and water ad libitum. The monkeys were observed twice daily for health status by the animal care and veterinary personnel.

Information on the animals and the samples used for analysis is presented in supplemental Table 1. Nine of the 12 animals were intravenously inoculated with stocks of SIVmac251. The 3 animals that developed SIVE and the 3 with chronic, untreated SIV infection (SIV-untreated group) were inoculated with an in vivo (rhesus monkey)

passaged stock from our laboratory,[29] the 3 with chronic SIV infection that were treated with antivirals to suppress viremia (SIV treated) were inoculated with an in vitro passaged stock (CEMx174 cells) provided by the Virus Characterization, Isolation and Production Core at Tulane National Primate Research Center (Covington, LA).[30] The antiviral-treated animals have been previously described.[7] Briefly, 5-weeks postinfection, they received a once-daily subcutaneous injection of 1 ml/kg of body weight containing 40 mg/ml emtricitabine (Gilead, Foster City, CA), 20 mg/ml tenofovir (Gilead), and 2.5 mg/ml dolutegravir (ViiV Healthcare Limited, Research Triangle, NC), continued until the time of necropsy. Necropsy plasma viral loads were determined by Seimens (Emeryville, CA) using a bDNA assay, or by SNB using quantitative reverse transcription-PCR (qRT-PCR) as previously described.[31]

At necropsy, deeply anesthetized (ketamine plus xylazine) animals were perfused intracardially with sterile PBS containing 1 U/ml heparin to clear blood and blood-borne cells from the brain vasculature. Brains were harvested for histopathology and molecular studies, and approximately half of the brain was then taken for microglia/macrophage isolation. Microglia/macrophage-enriched cellular isolation was performed using our previously described procedure.[28,32] In brief, a cellular preparation enriched in microglia and inflammatory cells were isolated by mechanical disruption, enzymatic digestions, and Percoll-gradient enrichment. These microglia/macrophage-enriched isolates were cryopreserved in 10% DMSO in FBS (Sigma–Aldrich, St. Louis, MO) and kept frozen at ≤140°C.

2.2 | scRNA-seq

Analysis of scRNA-seq data from 2 of the animals (21T and 34T, both from the SIVE group) were previously reported.[27] The methods used for these 2 and the other 10 samples were identical. The cryopreserved samples of enriched brain microglia/macrophages isolates were rapidly thawed in a 37°C water bath. Procedures were completed using our previously described methods.[27,28] Briefly, recovered cells were treated with 1% DNase (Sigma–Aldrich) followed by washing and then stained with UV-blue live/dead assay (Invitrogen, Waltham, MA). Cells were washed, resuspended in MACS separation buffer with 0.1% BSA, and incubated with NHP anti-CD11b microbeads (Miltenyi, Gladbach, Germany). Cells were washed and loaded onto MACS Separator LS columns, from which the positively selected CD11b cells were collected. These CD11b-enriched isolates were then stained with Brilliant Violet 605-labeled anti-mouse/human CD11b antibody clone M1/70 (BioLegend, San Diego, CA), washed, and sorted based on size, singlets, live, CD11b+ events using an Aria2 flow cytometer (BD Biosciences, San Diego, CA).

Post-sort, isolates were concentrated to approximately 1000 cells/μl, and assessed by trypan blue for viability and concentration. Based on 10× Genomics parameters targeting 8000 cells, the calculated volume of cells was loaded onto the 10× Genomics (Pleasanton, CA) Chromium GEM Chip and placed into Chromium Controller for cell capturing and library preparation. We used the 10× Genomics Single Cell 3′ GEM, Library, and Gel bead kit v3. The prepared libraries were then sequenced using an Illumina (San Diego, CA) Nextseq550 sequencer with the NSQ 500 hi-Output KT v2 (150 cycles).

2.3 | Data analysis

We performed demultiplexing and generating feature-cell matrices using 10× Genomics cellranger pipeline version 3.1.[29] Specifically, we used *cellranger mkfastq* to convert the raw base call (BCL) files from the Illumina Nextseq550 into FASTQ files. Then *cellranger count* aligned the reads to the customized combination reference genome of *Macaca mulatta* (Mmul10) and the SIV genome divided into 5 regions (based on NCBI reference sequences M22262.1).[27] *Cellranger count* also performed filtering, barcode counting, and unique molecular identifier (UMI) counting. As a result, a feature-cell matrix is created for each sample. An average of 5236 cells were identified per animal. DoubletFinder [30] was used on these matrices, eliminating 3222 of the 64,146 cells (5%) as doublets from the downstream analysis.

Partek (St. Louis, MO) Flow version 10.0 was used for in-depth analysis. Single-cell QA/QC was performed to filter out cells with low quality on the total UMI (<400 or >20,000), gene count per cell (<300 or >5000), and Mitochondrial UMI proportion (> 15%), 837 cells were removed from this step (1.3% of the starting pool of cells). The genes with maximal expression ≤1 were then removed. The remaining genes were filtered using a stringent rhesus monkey to human gene-mapping list, extracted from Biomart [56,57] with a confidence score equal to 1 and alignment coverage over 75%. Nonprotein coding genes were removed, in addition to genes that coded for ribosomal proteins and those from the mitochondrial genome. Normalization was performed using *scTransform*,[31] followed by principal component analysis (PCA) with the setting of 100 PCs for calculation. With the first 33 PCs, we performed graph-based clustering using the Louvain algorithm and a Euclidian distance metric, setting the resolution at 0.3, resulting in 10 clusters with a modularity of 0.98. Data visualization was performed using Uniform Manifold Approximation and Projection (UMAP), with a local neighborhood size of 15, a minimal distance of 0.1, Euclidean as the distance metric, and the first 33 PCs from PCA. For differentially enriched genes, ANOVA was performed (again using Partek software) using gene expression values that were normalized by converting the UMI to CPM (counts per million reads), then adding 1 and converting to the $\log_2$ value. Differentially expressed genes (DEGs) were defined as those with a false discovery rate of <0.05 and a fold change >|1.5|. The circos plot was generated using Metascape.[33]

For lists of the DEGs from the clusters generated above, we first converted them to human gene IDs, then performed ingenuity pathway analysis (IPA).[34] Canonical pathways, upstream regulators, biologic functions, and disease annotations were generated by the IPA and also overlaid the identified functional molecules with the networks.[35] *Z*-scores for IPA outputs were first filtered for missing values and

subsequently clustered hierarchically in Perseus v. 1.6.15.0 [36] using Euclidean distance calculations with linkage type set to average and no constraints. Preprocessing with *k*-means was selected, a maximum number of clusters and iterations were set at 300 and 10, respectively, with 1 allowed restart. Clustering was performed on both rows (regulator/pathway) and columns (graph-based cell cluster). Heatmaps were generated in GraphPad Prism version 9.3.1 for MacOs (GraphPad Software, San Diego, CA). To allow for better differentiation of color mapping, the maximum (red) and minimum (green) color values were applied to *Z*-scores greater than or equal to 3.0 and less than or equal −3.0, respectively.

2.4 | Original data availability

The scRNA-seq data from this study for the uninfected animals 16T, 38T, 41T; SIV-untreated animals 23T, 25T, 31T; SIV-treated animals 74T, 82T, and 83T; and SIVE animal 09T have been deposited in the NCBI GEO database, accession # GSE195574. Data from SIVE animals 17T and 34T, previously deposited in the NCBI GEO database, accession # GSE160384, was also used in this study.

2.5 | Online supplemental material

Five Excel workbooks are included in the online material. Table S1 contains the scRNA-seq metrics. Table S2 contains the up-regulated DEGs in nonmyeloid clusters 7 and 9 compared with the other clusters. Table S3 contains DEGs between conditions for clusters 4 and 5, and between all myeloid clusters. Table S4 contains the IPA canonical pathways for each myeloid cluster predicted by the DEGs. Table S5 contains the IPA upstream regulators for each myeloid cluster predicted by the DEGs.

3 | RESULTS

Cryopreserved enriched microglia/brain macrophage preparations were thawed, enriched by immunomagnetic selection for CD11b, and further purified by FACS to select for live, CD11b-positive cells. Cell suspensions were taken for capture using the 10× Genomics Chromium system. Data from 12 animals were studied, with 3 animals in each of the 4 groups. Details on the scRNA-seq metrics are provided in Table S1.

Quality assurance and quality control was performed on the cells identified as described in the *Methods*, from the 12 animals a total of 60,087 cells (an average of approximately 5000 cells per animal) were used in the subsequent analyses; we examined the expression of a curated list of rhesus protein-coding genes to which the SIV genome was added, resulting in 13,239 genes for analysis. Following normalization, we performed PCA and graph-based clustering. The conditions and clusters were visualized using UMAP. Cells from the 4 different conditions are largely grouped separately (Figure 1(A)). Ten graph-based clusters were found that identified different populations of cells (Figure 1(B)). Based on the DEGs, cluster 7 has the profile of cytotoxic T-lymphocytes and/or NK cells, whereas cluster 9 has the profile of endothelial and/or choroid plexus cells (Table S2). These cells were then removed from the analyses, leaving 56,088 cells expressing characteristic microglia/macrophage genes (Figure 1(C)) from the 4 conditions in 8 clusters for further analysis.

3.1 | Microglia/macrophages in each condition are made up of different proportions of defined cell clusters

Each condition has cells from multiple clusters, but their proportion varies with the condition as shown in the UMAP and pie chart in Figures 2(A) and 2(B)). Notably, each condition has the majority of the cells made up of just 1 cluster (uninfected: cluster 3, 65%; SIV-treated: cluster 2, 67%; SIVE: cluster 1, 77%) or at most 2 clusters (SIV-untreated: clusters 4 and 5, 47% and 35%, respectively) (Figure 2(B)). The SIVE condition contains all 8 clusters, whereas the other 3 conditions have 7, lacking cluster 10, which is only in SIVE. However, although containing 8 clusters, the makeup of the microglia/macrophages in SIVE is less diverse than in the other conditions. Shannon entropy can be used to calculate a diversity index (*H*, the larger the number, the more diverse),[37] revealing the condition with the highest diversity of cell distribution in the clusters is SIV treated, followed by uninfected, SIV treated, and SIVE ($H = 1.84$, 1.44., 1.20, and 1.10, respectively).

In order to better characterize the cells in the clusters, we examined expression of genes known to be expressed in myeloid cells. Other studies have characterized microglia, CAM, and monocytes in the brain and their activation and disease-induced changes, based on patterns of gene expression.[38–42] We examined the expression of myeloid genes that can characterize such cells (Figure 3). Microglia homeostatically express a number of genes that are also expressed as well in other myeloid cells, such as allograft inflammatory factor 1 (AIF1, a.k.a. Iba-1), CD14 (LPS coreceptor), and CSF1R (the macrophage CSF receptor). Expression of the purinergic receptor P2RY12 is thought to be highly specific for microglia, and expression of the lysophosphatidylserine receptor, GPR34, is highly enriched in microglia. P2RY12 is known to be down-regulated in microglial activation. The cells in clusters 2 and 3 express high levels of the above genes, whereas P2RY12 and GPR34 are lower in other clusters. They are still expressed in clusters 6, 1, 10, and 5, but not in clusters 4 and 8.

Clusters 4 and 8 also express lower levels of the complement genes C1QB and C3, both of which are typically expressed in microglia. Cluster 8 has a unique expression of ficolin 1 (FCN1) as well as S100A8 and S100A9 (a.k.a. MRP8 and MRP14), which are highly expressed in monocytes, and S100A8/9 expression characterizes recently emigrated monocytes from the bloodstream into the brain.[43] Furthermore cluster 8 has high expression of CD163, which is found on

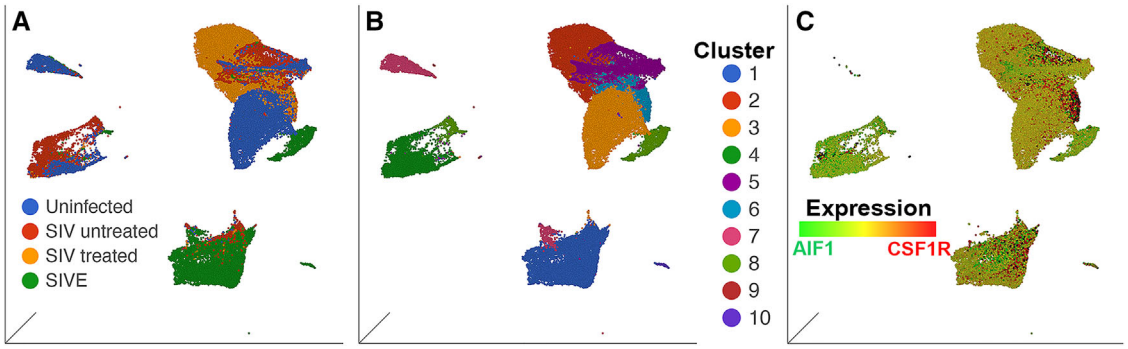

FIGURE 1 UMAP visualizations of scRNA-seq data. (A) Showing all cells following QA/QC, normalization, and filtering with the annotated gene list. Cells from the monkeys in the different conditions are designated by different colors. (B) as in (A), but with cells from the different graph-based clusters designated by different colors. (C) As in (A), but cluster 7 (CTL and NK cells) and cluster 9 (endothelial cells) removed and colored by the expression of myeloid genes AIF1 and CSF1R

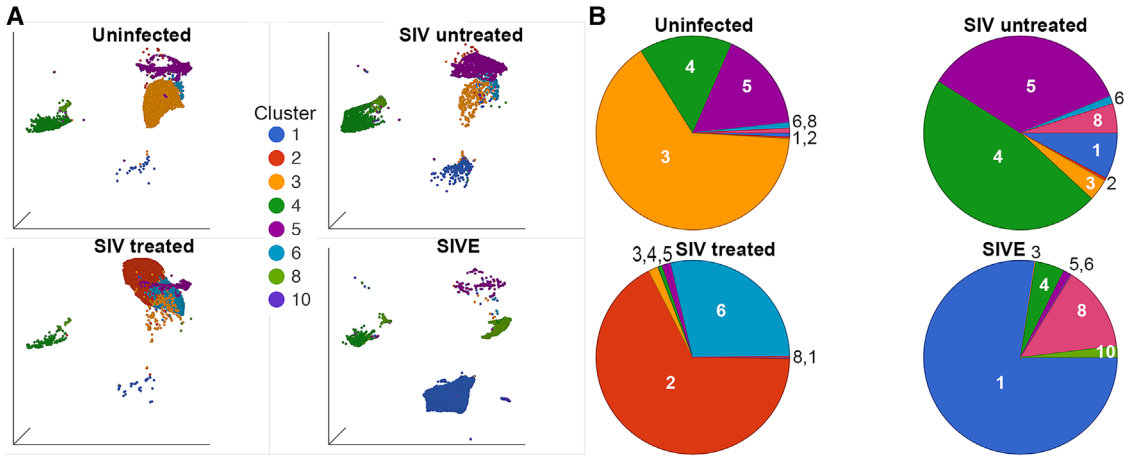

FIGURE 2 Different conditions are made up of different clusters of cells. (A) UMAP visualization of brain myeloid cell sc-RNAseq (excluding clusters 7 and 9), split to show cells from the different conditions, colored by graph-based clusters. (B) Pie charts with areas proportional to the percentage of cells in each condition from the different graph-based clusters of brain myeloid cell sc-RNAseq

perivascular macrophages in the brain.[44] Interestingly cluster 8 also has high expression of SPI1 (the transcription factor PU.1) critical in myeloid gene expression and present at high levels in monocytes, as well as CD68, and class II related genes (MAMU-DR and CD74) which characterize perivascular macrophages in the brain.[45] This is all consistent with cluster 8 representing macrophages (and/or recently emigrated monocytes) into a proinflammatory environment in the SIV-untreated and SIVE conditions. This cluster contains a relatively high proportion of the cells found in SIVE (14.3%), and SIV untreated (4.9%), with low levels in uninfected (0.8%) and SIV treated (0.2%)

In addition to cluster 8, clusters 1, 4, 5, and 10 express high levels of the MHC class II molecule MAMU-DRA and the MHC class II invariant chain CD74, indicating a function in antigen presentation, and for microglial activation. In addition to the class II molecules, clusters 1 and 10 are also notable for high expression of SPP1 (osteopontin) and apolipoprotein C1 (APOC1), which combined with the decreased P2RY12/GPR34 expression points to their activation, consistent with their predominance in SIVE. Similarly, the high expression of P2RY12/GPR34, with low expression of the MHC class II molecules and SPP1/APOC1 supports clusters 2 and 3 being in a homeostatic resting state. Although cluster 6 has lower P2RY12 expression, combined with the other markers it is likely in a similar state. This is consistent with clusters 2, 3, and 6 being predominant in the uninfected and SIV-treated conditions.

Clusters 4 and 5 are more difficult to classify, as they are present along with the predominant cluster 3, in the uninfected condition, and together they are dominant in the SIV-untreated condition. Both clusters 4 and 5 appear active in antigen presentation, with increased levels of the MHC class II molecule MAMU-DRA and the MHC class II invariant chain CD74. Cluster 4 resembles cluster 8 in much of the gene expression patterns, however with lower CD14, TLR4 (the LPS receptor), and FCN1, and lack of expression of S100A8/A9 and CD163. Cluster 5 is also related to cluster 8 in gene expression and has the unique (albeit low-level) expression of COLEC12, a C-lectin family scavenger receptor which is found in macrophages and

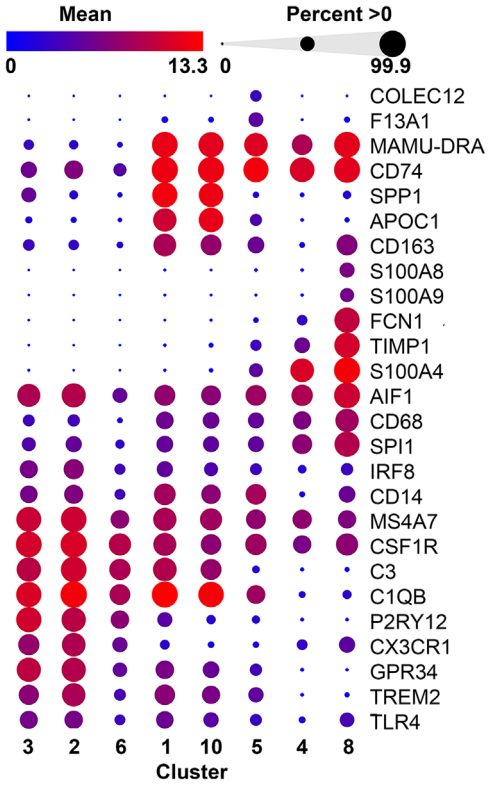

FIGURE 3 Expression of myeloid cell genes graph-based clusters. In the bubble plot, the size of the circles represents the percentage of cells in the cluster expressing the indicated gene, and the color represents the level of expression

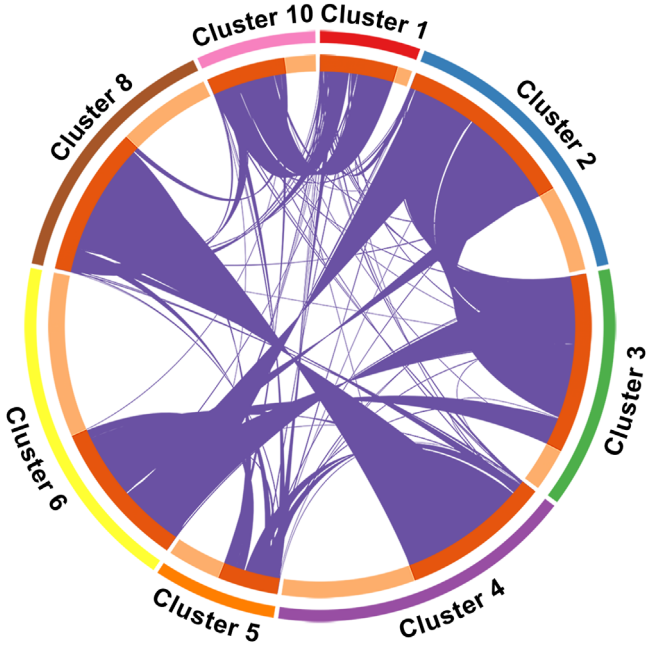

FIGURE 4 Relatedness of up-regulated genes. The circos plot shows the up-regulated genes within each cluster that are shared with other clusters (dark orange) and those that are unique to that cluster (light orange). The purple chords connect the clusters sharing up-regulated genes

activated microglia, as well as expressing Coagulation Factor XIII A Chain (F13A1), again found in macrophages.

Although clusters 4 and 5 are present in both the uninfected and SIV-untreated conditions, they may still differ in the expression of informative genes. Therefore, we performed ANOVA comparing cells in these clusters, separately, between the SIV-untreated and uninfected conditions (Table S3(A)). While similar in the graph-based clustering, it is notable that there are many genes associated with responsiveness to IFN, for example IFN alpha inducible protein 27 (IFI27) is increased 26-fold and 90-fold in SIV untreated versus uninfected in clusters 4 and 5, respectively. Similarly, apolipoprotein B mRNA editing enzyme catalytic subunit 3A (APOBEC3A) is increased 15-fold and 27-fold, and IFN-stimulated gene 15 (ISG15) is increased 8.3-fold and 6.2-fold. Thus, while present in both conditions, the clusters 4 and 5 are more activated in the SIV-untreated condition than their counterparts in the uninfected condition.

To further explore the relationships between the clusters we examined the commonalities in the up-regulated DEGs in the different clusters (Table S3(B)). As shown in the circos plot (Figure 4), consistent with the findings above, clusters 2 and 3 share many up-regulated DEGs with each other and with cluster 6, again characterizing the uninfected and SIV-treated groups. Similarly, clusters 1 and 10 (SIVE) share many genes with increased expression, as do clusters 4 and 8. The shared up-regulated genes in cluster 5 were dispersed throughout the other clusters.

3.2 | Infected cells are predominantly found in animals with encephalitis

To assess CNS infection, SIV-positive cells were identified as cells containing transcripts from the SIV genome. As expected, none were detected in the uninfected condition, and none were found in the SIV-treated condition. Two SIV-positive cells (0.02%) were found in the SIV-untreated condition, and many (9.2%) were present in the SIVE condition (Figure 5(A)). The clustering was consistent with this (Figure 5(B)), as cells from SIVE being largely in cluster 1 (the majority cluster in SIVE), which has the largest number of infected cells, with 6.1% of all cluster 1 cells expressing SIV transcripts (and of the SIVE cells in cluster 1, 6.5% are infected). The second-largest group of cells in SIVE was found in cluster 8 (which is the second-largest cluster located in SIVE), in which 8.1% are infected (and of the SIVE cells in cluster 8, 10.3% are infected). Intriguingly, cluster 10, found exclusively in SIVE, has 100% of the cells expressing SIV transcripts. These cells also expressed higher levels of transcripts from all regions of the SIV genome, including the *gag-pol* region, which is only found in full-length viral transcripts (Figure 5(C)). For the 2 infected cells in the SIV-untreated group, 1 is in cluster 4, and the other in cluster 5 (arrows, Figures 5(A) and 5(B)). These 2 clusters together contained the majority of the cells in the SIV-untreated condition.

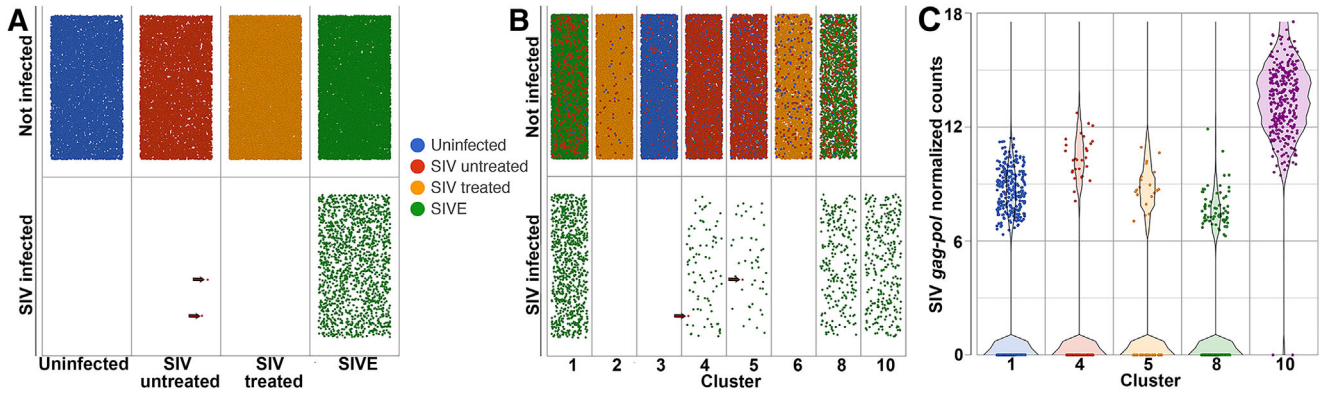

FIGURE 5 Identification of SIV-infected cells. (A) Dot plot of cells without SIV transcripts (not infected) and those with transcripts from the SIV genome (SIV infected), separated by, and colored by, condition. The 2 infected cells in SIV untreated are indicated by arrows. (B) As in (A), except separated by graph-based cluster. (C) Dot plot overlayed upon violin plot showing cells expressing SIV RNA from the *gag-pol* region (indicated full-length transcript), separated by, and colored by, graph-based cluster

These clusters also contain infected cells from the SIVE group (1.1 and 0.8% of all cells in the cluster, and 10.5 and 20.2% of the cells from the SIVE group expressing SIV transcripts, respectively).

3.3 | Pathway analyses indicate similarities between uninfected and SIV-treated conditions, and a common cluster of cells shared between SIV-untreated and SIVE

IPA was employed on DEGs for each cluster to gain insight into functional differences between the cell clusters. We first assessed alterations in canonical pathways (Table S4(A)). In total, 355 pathways were identified, of which 193 were present in each of the 8 clusters (Table S4(B) and Figure 6). Notably, several of the canonical pathways that exhibited the greatest range among clusters are associated with immune response and inflammation, including "interferon signaling" and "role of hypercytokinemia/hyperchemokinemia in the pathogenesis of influenza", which are increased in SIVE-associated clusters 1 and 10, SIVE and SIV-untreated-associated cluster 8, and decreased in uninfected- and SIV-treated-associated clusters 2, 3, and 6. Conversely, "MSP-RON signaling in macrophages pathway" as well as "G-protein coupled receptor signaling," are both increased in uninfected- and SIV-treated-associated clusters 2, 3, and 6, and decreased in SIVE-associated clusters 1 and 10, and SIV-untreated-associated cluster 8. Euclidean hierarchical clustering (with average linkage) revealed that based on the 193 common canonical pathways, clusters 2, 3, and 6 were closely related (uninfected- and SIV-treated associated), as were clusters 1 and 10 (all SIVE associated), as well as clusters 4 and 8 (which diverge in their linkage, with cluster 8 found in SIV untreated and SIVE, whereas cluster 4 is found predominantly in uninfected and SIV untreated). Cluster 5 (uninfected and SIV untreated) was more distantly connected to the clusters 1 and 10 grouping.

Next, we again used IPA to predict classes of "upstream regulators" based on the DEGs. We focused on 3 classes likely involved in

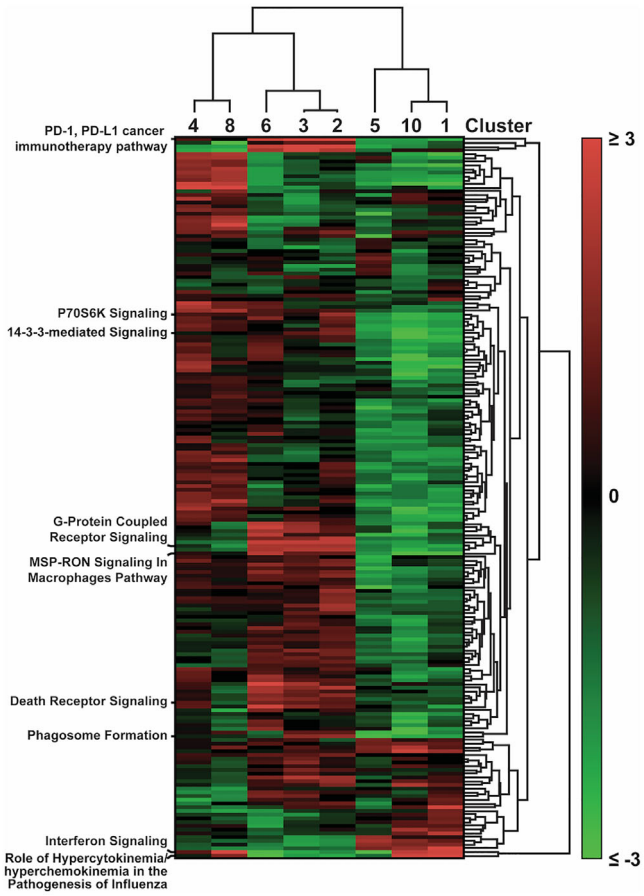

FIGURE 6 Cluster analysis of canonical IPA pathways. Euclidean clustering of activation *Z*-scores for canonical IPA pathways in each graph-based cell cluster is represented in the heatmap. Dendrograms illustrate the linkage relationships and distances between rows (pathways) and columns (graph-based cell clusters)

regulation in general (transcriptional regulation), neuroinflammation (cytokine), and neuroprotection, cell survival, and signal transduction (growth factor). We again used hierarchically clustering on the IPA-determined activation *Z*-scores, as shown in Figures 7(A)–7(C).

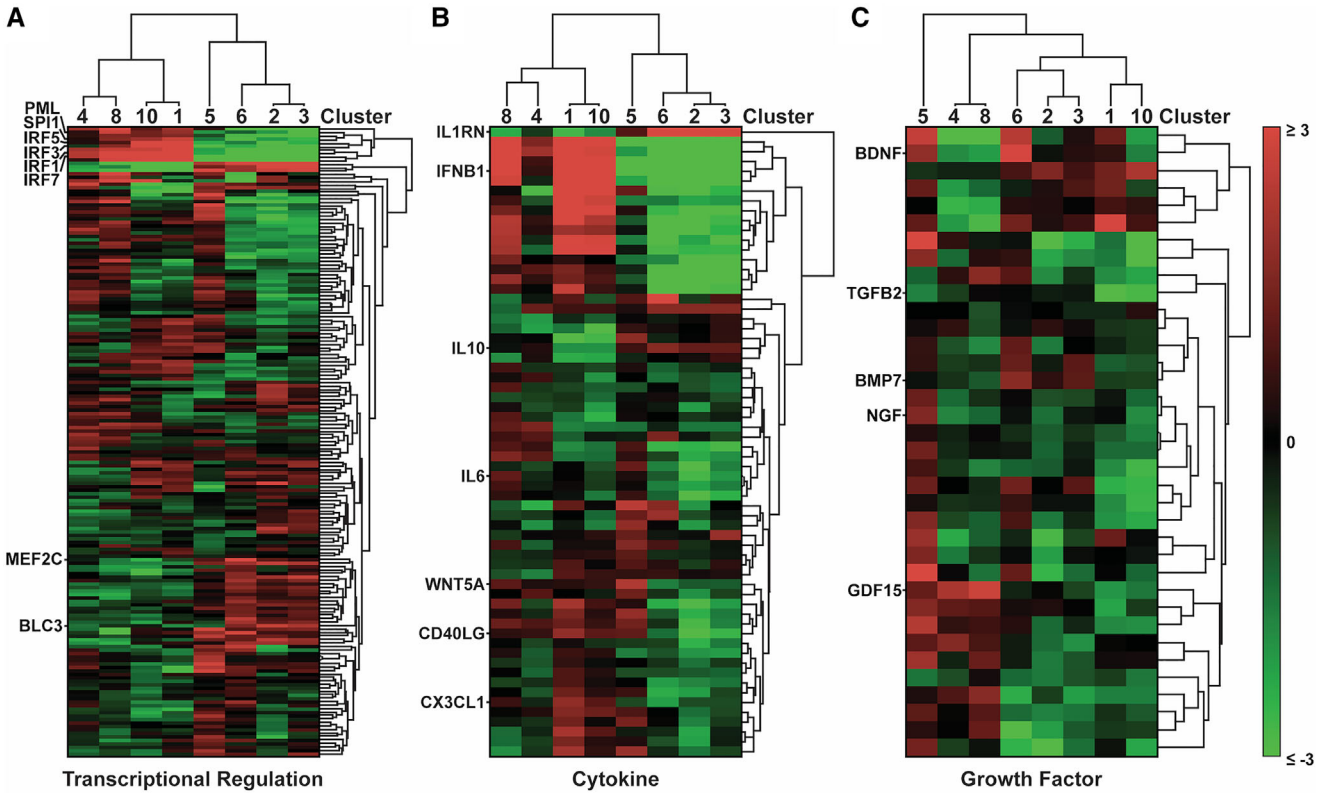

FIGURE 7 IPA reveals upstream regulators linked to infection status. Euclidean clustering of activation *Z*-scores in each graph-based cell cluster are represented in the heatmaps for upstream regulator classes (A) general regulation (transcriptional regulation), (B) neuroinflammation (cytokine), and (C) neuroprotection, cell survival, and signal transduction (growth factor). Dendrograms illustrate the linkage relationships and distances between rows (upstream regulator) and columns (graph-based cell clusters)

Complete lists of shared regulators used for clustering analysis in each class and their numerical *Z*-scores are available in Tables S5(A)–S5(C). Interestingly, clusters 2 and 3 were closely linked and grouped together with cluster 6, in all 3 classes of regulators, as was observed in the canonical pathways in Figure 6. Again, these clusters are composed primarily of cells from uninfected (cluster 3), and SIV-infected cART-suppressed (clusters 2 and 6) conditions, suggesting that cART treatment restores a more naïve-like gene expression profile in the microglia. The clusters primarily from SIVE also cluster together (clusters 1 and 10), again as in the canonical pathways, with clusters 4 and 8 (the latter in the SIVE and SIV-untreated groups) linked together and are related to clusters 1 and 10 for transcriptional regulators and cytokines, but not growth factors. Cluster 5 varied in its linkage.

In further support of viral suppression restoring a more naïve (i.e. similar to the uninfected condition) transcriptional program, we observed converse activation scores of transcriptional regulators involved inflammation and immune response (IFN response factor, IRF, IRF-1/3/5/7),[46] a key factor in the activation of myeloid development and gene expression profiles (Spi-1-proto-oncogene, SPI1, a.k.a. PU.1),[47] and another involved in antiviral responses to IFN signaling (promyelocytic leukemia protein).[48] These increased in clusters comprised of primarily SIVE/SIV-untreated clusters [1,8,10] and decreased in clusters comprised of uninfected/SIV-treated groups.[2,3,6] In contrast, the activity of myocyte-specific enhancer factor 2C (MEF2C), which is known to suppress the microglial inflammatory response,[49] is increased in clusters comprised of uninfected/SIV-treated groups [2,3,6] and decreased in clusters comprised of SIVE/SIV.[1,8,10]

Consistent with this, we also observed corroboration in activation scores for cytokines representing pro- and anti-inflammatory activities between SIVE/SIV-untreated and uninfected/SIV-treated conditions, respectively. This is exemplified by high IFN beta 1 (IFNB1) activity, and low activity for IL-1 receptor antagonist (IL1RN) in SIVE- and SIV-untreated-associated clusters, versus uninfected- and SIV-treated-associated clusters, with low IFNB1 and high IL1RN. Fractalkine (CX3CL1), which is the ligand for CX3CR1, a characteristic gene expressed in macrophages, serves to maintain microglia in a relatively quiescent state.[50] CX3CL1 expression is high in uninfected- and SIV-treated-associated clusters, whereas low in SIVE- and SIV-untreated-associated clusters. In our analysis of growth factors, we did not observe stark converse relationships of activation scores distinguishing the clusters found in the related conditions, as above.

4 | DISCUSSION

Although modern therapies like cART have transformed HIV from a lethal disease to a manageable condition, associated neurocognitive consequences remain a concern.[51] Paradoxically, microglia and macrophages, which comprise the innate defense system in the brain

and are crucial for CNS homeostasis, are targets for HIV and key players in its neuropathogenesis.[52,53] In addition, these infected cells can serve as viral reservoirs even with effective treatment.[54] Here, using an scRNA-seq approach in the SIV-NHP model, we demonstrate differential transcriptional programs in brain myeloid cells from monkeys under 4 conditions: uninfected, SIV-infected without treatment (SIV untreated), SIV infected, cART treated to suppress viremia (SIV treated), and SIV infected with SIVE. Our study revealed alterations in composition (both lineage and gene expression profiles) of the cell populations between groups that could be helpful as both therapeutic targets and biomarkers.

As expected, we observed greater expression of SIV transcripts correlating with infection severity (SIVE > SIV untreated), and lack of such transcripts in SIV-infected cART-treated, or uninfected, monkeys. Notably, we only detected 2 SIV-expressing cells in SIV-untreated animals. While our analysis detects viral transcripts, the sensitivity of scRNA-seq is limiting, thus it is possible that cells expressing low amounts of viral RNA cloud be missed. However, we note that in a model of accelerated simian AIDS, animals without CNS disease had low to undetectable levels of SIV RNA, and the majority did not have detectable productively infected CD11b+ cells (microglia or macrophages) in the brain.[55] Using the same model system with the addition of suppressive antiretroviral treatment, it was found that SIV RNA was not detected in the brains of the SIV-infected monkeys, although provirus was found, and the cells could serve as a reservoir capable of producing virus, with a median of 0.268 infectious cells per million CD11b+ brain cells.[8] Similarly, in our prior study that included these 3 treated, virally suppressed animals and 2 additional treated animals, we found 0.18 infectious cells per million CD11b+ brain cells.[7]

Viral suppression by treatment also resulted in gene expression profiles similar to those observed in uninfected monkeys and distinct from those seen with active untreated infection. In line with this, several genes with relevant immune functions were differentially expressed in uninfected and SIV-treated conditions compared with SIVE/SIV-untreated groups. Examples represent functions in antigen presentation: CD74, MAMU-DRA; scavenging and immune recruitment: CXC3R1, CD68, CD163; inflammation: IRF8; transcriptional regulation: SP1, TAL1; antiapoptotic signaling and survival: CX3CR1, SPP1; and receptor signaling: MERTK, P2RY12, GPR34. Key biologic pathways and upstream regulators identified by IPA, exhibited similar inverse relationships between uninfected/SIV-treated and SIVE/SIV-untreated groups that were supported by cluster analysis. Among those associated with viral immune response were IFN signaling and response factors, excessive cytokine and chemokine release, immune suppression, scavenging and clearance, and proliferation/death signaling.

4.1 | Myeloid diversity is influenced by SIV and cART

CNS myeloid diversity under homeostatic states is composed primarily of surveillant microglia and perivascular macrophages, which rapidly shift into states of immune activation recruiting peripheral monocytes and activating resident microglia and macrophages.[56] Consistent with this, composition of graph-based clusters in our study varied between groups although some clusters were shared by more than 1 group. Correlating with a low level of infection and immune activation state, but without active disease, the greatest microglia/macrophage diversity was observed in SIV-infected animals not treated with cART. The condition of SIVE was the least diverse, likely due to general activation in encephalitis. The cells had a high level of infection, with cells in a highly activated state (clusters 1 and 10) and an increased proportion in cluster 8; the latter cluster shared largely with SIV-untreated and resembling activated monocyte/macrophages. In uninfected animals' cells, cluster 3 was most prevalent, while cART-treated infected animals' cells clusters 2 and 6 were prominent, and all 3 of these clusters were comprised of relatively quiescent cells. The reduced diversity in the treated group may relate to this overall quiescence. We cannot rule out an effect of the treatment itself on microglia, as an uninfected, cART-treated group was not examined. Interestingly, clusters 4 and 5 were shared between uninfected and SIV-untreated groups; however, within these clusters, differences were found pointing to microglial activation in the SIV-untreated group.

4.2 | cART restores a homeostatic naïve-like state

Microglia, the dominant immune cell type in the CNS, perform essential functions to maintain homeostatic balance in the CNS.[57] Among these are clearance of debris, synaptic pruning, regulation of dendritic spine density, synapse maturation, and regulation of neuronal activity. Homeostatic microglial states are defined by a core set of genes, including relatively high expression of P2RY12, TREM2, GPR34, and CX3CR1, comparable to the pattern we observed in uninfected animals (cluster 3).[58,59] Conversely, these genes are inhibited in activated states such as those in SIV untreated and SIVE. Notably, the overlap between the SIV-untreated and cART-suppressed (SIV treated) conditions was minimal, confirming lowered microglial activation and suggesting the restoration of a more naïve-like state. Indicative and consistent with reduced immune activation, the predominant clusters in cART suppressed animals (clusters 2 and 6) were similar in expression pattern and pathway activation to cluster 3. Specifically, P2RY12 expression was high in both clusters 2 and 3. A purinergic receptor, P2RY12, which in the peripherally is involved in platelet aggregation, is highly specific to surveillant state microglia in the brain, where it regulates recruitment of microglial processes to specialized purinergic junctions, neuronal–microglial communication, glutamatergic tone, and dendritic spine density.[60,61] TREM2, like P2RY12 functions in CNS homeostasis participating in surveillant microglial sensing, homeostatic clearance, and regulating microglia survival and proliferation [62] was also comparable between cluster 2 and 3. Notably, mutations or dysregulated expression of P2RY12 and TREM2 are associated with neurodegenerative disorders, including Alzheimer's disease.[63,64]

Correlating with gene expression programs and reduced inflammatory states, activation scores of pathways were comparable between clusters 2, 3, and 6. With an elevated activation score, the pathway

"MSP-RON signaling in macrophages pathway" regulates the immune state by reducing microglial inflammation, decreasing characteristics of the proinflammatory M1 state, and promoting an M2 phenotype.[65] Conversely, with reduced activation scores, the pathways of "interferon signaling," classically associated with proinflammatory response and "role of hypercytokinemia/hyperchemokinemia in the pathogenesis of influenza," colloquially known as cytokine storm, contribute to enhanced inflammation, glial activation, and chemotaxis.[66,67] The similar degrees of activation for these pathways in cART suppressed clusters in SIV treated [2 and 6] and cluster 3 in the uninfected condition reinforce the notion that cART restores a naïve-like state.

4.3 | SIVE is associated with robust inflammatory activation

As expected, in SIVE, increased populations of activated microglia and macrophages, as in clusters 1, 8, and 10, were coupled to high viral replication, elevated proinflammatory cytokine production, and numerous IFN-regulated genes. Many of these up-regulated effectors were similar to our prior profiling of SIVE and HIVE using gene arrays.[68,69] Clusters 1 and 10, which contained the highest percentage SIV transcript expressing cells and shared a large percentage of DEGs, exhibited proinflammatory activation of regulators and effector molecules (IRF1/3/5/7, IFNB1, IL6, and others) and associated pathways ("interferon signaling" and "role of hypercytokinemia/hyperchemokinemia in the pathogenesis of influenza").

Of additional interest as a biomarker was CD163, which is known to be expressed in microglia in SIVE and HIVE, as well as in perivascular macrophages.[44,70] Soluble CD163, released from activated monocytes, has been shown to be elevated in the blood during both SIV and HIV infection.[71,72] Furthermore, plasma CD163 correlates with neurocognitive impairment and neuropathology in PWH.[73,74] CD163 expression is high in clusters 1 and 10 (SIVE), at moderate levels in clusters 5 and 8 (SIV untreated as well as SIVE for cluster 8), and low in clusters 2, 3, and 6 (uninfected and SIV treated). Another potential biomarker identified was SPP1 (osteopontin), that was expressed at high levels in clusters 1 and 10 (SIVE). Plasma osteopontin levels are correlated with neurocognitive impairment in PWH [75] and its expression was increased in the brain and CSF of those with impairment.[76]

5 | SUMMARY

SIV infection of monkeys changes the makeup of microglia subsets in the brain. While high-level infection within the brain in SIVE leads to clusters of highly activated cells expressing inflammatory factors, even lower-level infection in infected but untreated animals changes the characteristics of microglia to an activated phenotype. Both SIVE and SIV-infected untreated animals share a higher proportion of macrophages within the brain myeloid cells. Microglia from SIV-infected animals that were treated with antivirals to effectively suppress viremia exhibited profiles of a homeostatic state similar to those seen in uninfected animals. Limitations of our study include the retrospective analysis of animals from different experiments, diverse times of cryopreservation storage, different passage history of infecting viral stocks (although of similar origin), small numbers of animals per group (3), a shorter infection time period than in PWH, and examination of microglia and macrophages but not other brain cells that could also contribute to alterations found with infection and its treatment. Furthermore, scRNA-seq captures only a fraction of the transcriptome of each cell, leading to data with zero inflation and subsequent false negatives.

In conclusion, our study provides an important perspective to the ongoing debate on microglia/macrophages as key target cells for SIV/HIV infection in the CNS and their role in pathogenesis, and underscores the need for in-depth analysis of more extensive studies.

ACKNOWLEDGMENTS

This work was supported by NIH grants P30MH062261 and R01DA043164. A. J. T. was supported by a UNMC Vice Chancellor for Research pilot grant associated with the Chronic HIV infection and Aging in NeuroAIDS Center. We thank Benjamin Lamberty, Katy Emanuel, Shannon Callen, and Kelsey Dyball for assistance with the NHP work and Greg Kubik, Alok Dhar, and Dr. Jim Eudy for scRNA-seq expertise. The UNMC DNA Sequencing Core receives support from NIH grants P20GM103427 and P30CA036727. The UNMC Flow Cytometry Research Facility receives state funds from the Nebraska Research Initiative and the NIH grant P30CA036727. Major instrumentation has been provided by the UNMC Office of the Vice Chancellor for Research, The University of Nebraska Foundation, the Nebraska Banker's Fund, and by the NIH Shared Instrument Program. This publication's contents are the sole responsibility of the authors and do not necessarily represent the official views of the funders.

AUTHORSHIP

Conceptualization: H. S. F., M. N., and B. M. *Investigation*: H. S. F., B. M., S. B., and S. N. B. *Data curation – formal analysis*: H. S. F., M. N., and A. J. T. *Writing – original draft*: A. J. T. *Writing – reviewing, editing and revision*: A. J. T., H. S. F., M. N., B. M., S. B., S. N. B., and C. G.

DISCLOSURE

The authors declare no financial conflicts of interest

REFERENCES

1. Burudi EME, Fox HS. Simian immunodeficiency virus model of HIV-induced central nervous system dysfuntion. In: Buchmeier MJ, Campbell I, eds. *Advances in virus research*. Academic Press; 2001:431-464.
2. Desrosiers RC. The simian immunodeficiency viruses. *Annu Rev Immunol*. 1990;8:557-578.
3. Fox HS, Gold LH, Henriksen SJ, Bloom FE. Simian immunodeficiency virus: a model for neuroAIDS. *Neurobiol Dis*. 1997;4:265-274. https://doi.org/10.1006/nbdi.1997.0159. Epub 1997/01/01. PubMed PMID: 9361303.
4. Lackner AA. Pathology of simian immunodeficiency virus induced disease. *Curr Top Microbiol Immunol*. 1994;188:35-164.

5. Zink MC, Spelman JP, Robinson RB, Clements JE. SIV infection of macaques–modeling the progression to AIDS dementia. *J Neurovirol*. 1998;4:249-259.
6. Abreu CM, Veenhuis RT, Avalos CR, et al. Infectious virus persists in CD4(+) T cells and macrophages in antiretroviral therapy-suppressed simian immunodeficiency virus-infected macaques. *J Virol*. 2019;93. https://doi.org/10.1128/JVI.00065-19. Epub 2019/05/24. PubMed PMID: 31118264; PMCID: PMC6639293.
7. Acharya A, Olwenyi OA, Thurman M, et al. Chronic morphine administration differentially modulates viral reservoirs in SIVmac251 infected rhesus macaque model. *J Virol*. 2020. https://doi.org/10.1128/JVI.01657-20. Epub 2020/12/18. PubMed PMID: 33328304; PMCID: PMC8092838.
8. Avalos CR, Abreu CM, Queen SE, et al. Brain macrophages in simian immunodeficiency virus-infected, antiretroviral-suppressed macaques: a functional latent reservoir. *MBio*. 2017;8. https://doi.org/10.1128/mBio.01186-17. Epub 2017/08/16. PubMed PMID: 28811349; PMCID: PMC5559639.
9. Mavigner M, Habib J, Deleage C, et al. Simian immunodeficiency virus persistence in cellular and anatomic reservoirs in antiretroviral therapy-suppressed infant rhesus macaques. *J Virol*. 2018;92. https://doi.org/10.1128/JVI.00562-18. Epub 2018/07/13. PubMed PMID: 29997216; PMCID: PMC6146711.
10. Rahman MA, Robert-Guroff M. Accelerating HIV vaccine development using non-human primate models. *Expert Rev Vaccines*. 2019;18:61-73. https://doi.org/10.1080/14760584.2019.1557521. Epub 2018/12/12. PubMed PMID: 30526159.
11. Martins MA, Watkins DI. What is the predictive value of animal models for vaccine efficacy in humans? Rigorous simian immunodeficiency virus vaccine trials can be instructive. *Cold Spring Harb Perspect Biol*. 2018;10. https://doi.org/10.1101/cshperspect.a029504. Epub 2017/03/30. PubMed PMID: 28348034.
12. Mallard J, Williams KC. Animal models of HIV-associated disease of the central nervous system. *Handb Clin Neurol*. 2018;152:41-53. https://doi.org/10.1016/B978-0-444-63849-6.00004-9. Epub 2018/04/02. PubMed PMID: 29604983.
13. Goulder P, Deeks SG. HIV control: is getting there the same as staying there? *PLoS Pathog*. 2018;14:e1007222. https://doi.org/10.1371/journal.ppat.1007222. Epub 2018/11/02. PubMed PMID: 30383857; PMCID: PMC6211749.
14. Estes JD, LeGrand R, Petrovas C. Visualizing the immune system: providing key insights into HIV/SIV infections. *Front Immunol*. 2018;9:423. https://doi.org/10.3389/fimmu.2018.00423. Epub 2018/03/20. PubMed PMID: 29552017; PMCID.
15. Joseph SB, Arrildt KT, Sturdevant CB, Swanstrom R. HIV-1 target cells in the CNS. *J Neurovirol*. 2015;21:276-289. https://doi.org/10.1007/s13365-014-0287-x. Epub 2014/09/23. PubMed PMID: 25236812; PMCID: PMC4366351.
16. Wallet C, De Rovere M, Van Assche J, et al. Microglial cells: the main HIV-1 reservoir in the brain. *Front Cell Infect Microbiol*. 2019;9:362. https://doi.org/10.3389/fcimb.2019.00362. Epub 2019/11/12. PubMed PMID: 31709195; PMCID: PMC6821723.
17. Gelman BB. Neuropathology of HAND with suppressive antiretroviral therapy: encephalitis and neurodegeneration reconsidered. *Curr HIV/AIDS Rep*. 2015;12:272-279. https://doi.org/10.1007/s11904-015-0266-8. Epub 2015/04/11. PubMed PMID: 25860316; PMCID: PMC4427627.
18. Heaton RK, Franklin DR, Ellis RJ, et al. HIV-associated neurocognitive disorders before and during the era of combination antiretroviral therapy: differences in rates, nature, and predictors. *J Neurovirol*. 2011;17:3-16. https://doi.org/10.1007/s13365-010-0006-1. Epub 2010/12/22. PubMed PMID: 21174240; PMCID: PMC3032197.
19. Heaton RK, Clifford DB, Franklin DR, et al. HIV-associated neurocognitive disorders persist in the era of potent antiretroviral therapy: cHARTER Study. *Neurology*. 2010;75:2087-2096. https://doi.org/10.1212/WNL.0b013e318200d727. PubMed PMID: 21135382; PMCID: 2995535.
20. Everall I, Vaida F, Khanlou N, et al. National Neuro ATC. Cliniconeuropathologic correlates of human immunodeficiency virus in the era of antiretroviral therapy. *J Neurovirol*. 2009;15:360-370. https://doi.org/10.3109/13550280903131915. Epub 2010/02/24. PubMed PMID: 20175693; PMCID: PMC3078805.
21. Clifford DB. HIV-associated neurocognitive disorder. *Curr Opin Infect Dis*. 2017;30:117-122. https://doi.org/10.1097/QCO.0000000000000328. Epub 2016/11/01. PubMed PMID: 27798498; PMCID: PMC5382956.
22. Sillman B, Woldstad C, McMillan J, Gendelman HE. Neuropathogenesis of human immunodeficiency virus infection. *Handb Clin Neurol*. 2018;152:21-40. https://doi.org/10.1016/B978-0-444-63849-6.00003-7. Epub 2018/04/02. PubMed PMID: 29604978.
23. AAN. Nomenclature and research case definitions for neurologic manifestations of human immunodeficiency virus-type 1 (HIV-1) infection. Report of a Working Group of the American Academy of Neurology AIDS Task Force. *Neurology*. 1991;41:778-785. Epub 1991/06/01. https://doi.org/10.1212/wnl.41.6.778. PubMed PMID: 2046917.
24. Antinori A, Arendt G, Becker JT, et al. Updated research nosology for HIV-associated neurocognitive disorders. *Neurology*. 2007;69:1789-1799. https://doi.org/10.1212/01.WNL.0000287431.88658.8b. Epub 2007/10/05. PubMed PMID: 17914061; PMCID: PMC4472366.
25. Alliot F, Godin I, Pessac B. Microglia derive from progenitors, originating from the yolk sac, and which proliferate in the brain. *Brain Res Dev Brain Res*. 1999;117:145-152. https://doi.org/10.1016/s0165-3806(99)00113-3. Epub 1999/11/24. PubMed PMID: 10567732.
26. Goldmann T, Wieghofer P, Jordao MJ, et al. Origin, fate and dynamics of macrophages at central nervous system interfaces. *Nat Immunol*. 2016;17:797-805. https://doi.org/10.1038/ni.3423. Epub 2016/05/03. PubMed PMID: 27135602; PMCID: PMC4968048.
27. Niu M, Morsey B, Lamberty BG, et al. Methamphetamine increases the proportion of SIV-infected microglia/macrophages, alters metabolic pathways, and elevates cell death pathways: a single-cell analysis. *Viruses*. 2020;12. https://doi.org/10.3390/v12111297. Epub 2020/11/18. PubMed PMID: 33198269; PMCID: PMC7697917.
28. Morsey B, Niu M, Dyavar SR, et al. Cryopreservation of microglia enables single-cell RNA sequencing with minimal effects on disease-related gene expression patterns. *iScience*. 2021;24:102357. https://doi.org/10.1016/j.isci.2021.102357. Epub 2021/04/20. PubMed PMID: 33870145; PMCID: PMC8044433.
29. Burdo TH, Marcondes MC, Lanigan CM, Penedo MC, Fox HS. Susceptibility of Chinese rhesus monkeys to SIV infection. *AIDS*. 2005;19:1704-1706. https://doi.org/10.1097/01.aids.0000186823.76230.33. Epub 2005/09/27. PubMed PMID: 16184046.
30. Del Prete GQ, Scarlotta M, Newman L, et al. Comparative characterization of transfection- and infection-derived simian immunodeficiency virus challenge stocks for in vivo nonhuman primate studies. *J Virol*. 2013;87:4584-4595. https://doi.org/10.1128/JVI.03507-12. Epub 2013/02/15. PubMed PMID: 23408608; PMCID: PMC3624367.
31. Byrareddy SN, Kallam B, Arthos J, et al. Targeting alpha4beta7 integrin reduces mucosal transmission of simian immunodeficiency virus and protects gut-associated lymphoid tissue from infection. *Nat Med*. 2014;20:1397-1400. https://doi.org/10.1038/nm.3715. Epub 2014/11/25. PubMed PMID: 25419708; PMCID: PMC4257865.
32. Marcondes MC, Burudi EM, Huitron-Resendiz S, et al. Highly activated CD8(+) T cells in the brain correlate with early central nervous system dysfunction in simian immunodeficiency virus infection. *J Immunol*. 2001;167:5429-5438. https://doi.org/10.4049/jimmunol.167.9.5429. Epub 2001/10/24. PubMed PMID: 11673562.
33. Zhou Y, Zhou B, Pache L, et al. Metascape provides a biologist-oriented resource for the analysis of systems-level datasets. *Nat Commun*. 2019;10:1523. https://doi.org/10.1038/s41467-019-09234-6. Epub 2019/04/05. PubMed PMID: 30944313; PMCID: PMC6447622.

34. QIAGEN. Ingenuity Pathway Analysis [cited 2021 December 15, 2021]. Available from: https://digitalinsights.qiagen.com/IPA
35. Kramer A, Green J, Pollard J Jr, Tugendreich S. Causal analysis approaches in ingenuity pathway analysis. *Bioinformatics*. 2014;30:523-530. https://doi.org/10.1093/bioinformatics/btt703. Epub 2013/12/18. PubMed PMID: 24336805; PMCID: PMC3928520.
36. Tyanova S, Temu T, Sinitcyn P, et al. The Perseus computational platform for comprehensive analysis of (prote)omics data. *Nat Methods*. 2016;13:731-740. https://doi.org/10.1038/nmeth.3901. Epub 2016/06/28. PubMed PMID: 27348712.
37. Shannon CE. A mathematical theory of communication. *Bell System Technical Journal*. 1948;27:379-423. https://doi.org/10.1002/j.1538-7305.1948.tb01338.x
38. Sun J, Song Y, Chen Z, et al. Heterogeneity and molecular markers for CNS glial cells revealed by single-cell transcriptomics. *Cell Mol Neurobiol*. 2021. https://doi.org/10.1007/s10571-021-01159-3. Epub 2021/10/28. PubMed PMID: 34704168.
39. Masuda T, Sankowski R, Staszewski O, Prinz M. Microglia heterogeneity in the single-cell era. *Cell Rep*. 2020;30:1271-1281. https://doi.org/10.1016/j.celrep.2020.01.010. Epub 2020/02/06. PubMed PMID: 32023447.
40. Kubick N, Henckell Flournoy PC, Klimovich P, Manda G, Mickael ME. What has single-cell RNA sequencing revealed about microglial neuroimmunology? *Immun Inflamm Dis*. 2020;8:825-839. https://doi.org/10.1002/iid3.362. Epub 2020/10/22. PubMed PMID: 33085226; PMCID: PMC7654416.
41. Gerrits E, Heng Y, Boddeke E, Eggen BJL. Transcriptional profiling of microglia; current state of the art and future perspectives. *Glia*. 2020;68:740-755. https://doi.org/10.1002/glia.23767. Epub 2019/12/18. PubMed PMID: 31846124; PMCID: PMC7064956.
42. Dubbelaar ML, Kracht L, Eggen BJL, Boddeke E. The kaleidoscope of microglial phenotypes. *Front Immunol*. 2018;9:1753. https://doi.org/10.3389/fimmu.2018.01753. Epub 2018/08/16. PubMed PMID: 30108586; PMCID: PMC6079257.
43. Soulas C, Conerly C, Kim WK, et al. Recently infiltrating MAC387(+) monocytes/macrophages a third macrophage population involved in SIV and HIV encephalitic lesion formation. *Am J Pathol*. 2011;178:2121-2135. https://doi.org/10.1016/j.ajpath.2011.01.023. Epub 2011/04/26. PubMed PMID: 21514427; PMCID: PMC3081227.
44. Kim WK, Alvarez X, Fisher J, et al. CD163 identifies perivascular macrophages in normal and viral encephalitic brains and potential precursors to perivascular macrophages in blood. *Am J Pathol*. 2006;168:822-834. PubMed PMID: 16507898.
45. Bottcher C, Schlickeiser S, Sneeboer MAM, et al. Human microglia regional heterogeneity and phenotypes determined by multiplexed single-cell mass cytometry. *Nat Neurosci*. 2019;22:78-90. https://doi.org/10.1038/s41593-018-0290-2. Epub 2018/12/19. PubMed PMID: 30559476.
46. Jefferies CA. Regulating IRFs in IFN driven disease. *Front Immunol*. 2019;10:325. https://doi.org/10.3389/fimmu.2019.00325. Epub 2019/04/16. PubMed PMID: 30984161; PMCID: PMC6449421.
47. Yeh H, Ikezu T. Transcriptional and epigenetic regulation of microglia in health and disease. *Trends Mol Med*. 2019;25:96-111. https://doi.org/10.1016/j.molmed.2018.11.004. Epub 2018/12/24. PubMed PMID: 30578089; PMCID: PMC6377292.
48. Kim YE, Ahn JH. Positive role of promyelocytic leukemia protein in type I interferon response and its regulation by human cytomegalovirus. *PLoS Pathog*. 2015;11:e1004785. https://doi.org/10.1371/journal.ppat.1004785. Epub 2015/03/27. PubMed PMID: 25812002; PMCID: PMC4374831.
49. Deczkowska A, Matcovitch-Natan O, Tsitsou-Kampeli A, et al. Mef2C restrains microglial inflammatory response and is lost in brain ageing in an IFN-I-dependent manner. *Nat Commun*. 2017;8:717. https://doi.org/10.1038/s41467-017-00769-0. Epub 2017/09/30. PubMed PMID: 28959042; PMCID: PMC5620041.
50. Pawelec P, Ziemka-Nalecz M, Sypecka J, Zalewska T. The impact of the CX3CL1/CX3CR1 axis in neurological disorders. *Cells*. 2020;9. https://doi.org/10.3390/cells9102277. Epub 2020/10/18. PubMed PMID: 33065974; PMCID: PMC7600611.
51. Wei J, Hou J, Su B, et al, The prevalence of frascati-criteria-based HIV-associated neurocognitive disorder (HAND) in HIV-infected adults: a systematic review and meta-analysis. *Front Neurol*. 2020;11:581346. Epub 2020/12/19. https://doi.org/10.3389/fneur.2020.581346. PubMed PMID: 33335509; PMCID: PMC7736554.
52. Cornell J, Salinas S, Huang HY, Zhou M. Microglia regulation of synaptic plasticity and learning and memory. *Neural Regen Res*. 2022;17:705-716. https://doi.org/10.4103/1673-5374.322423. Epub 2021/09/03. PubMed PMID: 34472455; PMCID: PMC8530121.
53. Borrajo Lopez A, Penedo MA, Rivera-Baltanas T, et al. Microglia: the real foe in HIV-1-associated neurocognitive disorders? *Biomedicines*. 2021;9. https://doi.org/10.3390/biomedicines9080925. Epub 2021/08/28. PubMed PMID: 34440127; PMCID: PMC8389599.
54. Mohammadzadeh N, Roda W, Branton WG, et al. Lentiviral infections persist in brain despite effective antiretroviral therapy and neuroimmune activation. *mBio*. 2021;12:e0278421. https://doi.org/10.1128/mBio.02784-21. Epub 2021/12/15. PubMed PMID: 34903055; PMCID: PMC8669467.
55. Avalos CR, Price SL, Forsyth ER, et al. Quantitation of productively infected monocytes and macrophages of simian immunodeficiency virus-infected macaques. *J Virol*. 2016;90:5643-5656. https://doi.org/10.1128/JVI.00290-16. Epub 2016/04/01. PubMed PMID: 27030272; PMCID: PMC4886778.
56. Herz J, Filiano AJ, Smith A, Yogev N, Kipnis J. Myeloid cells in the central nervous system. *Immunity*. 2017;46:943-956. https://doi.org/10.1016/j.immuni.2017.06.007. Epub 2017/06/22. PubMed PMID: 28636961; PMCID: PMC5657250.
57. Li Q, Barres BA. Microglia and macrophages in brain homeostasis and disease. *Nat Rev Immunol*. 2018;18:225-242. https://doi.org/10.1038/nri.2017.125. Epub 2017/11/21. PubMed PMID: 29151590.
58. Patir A, Shih B, McColl BW, Freeman TC. A core transcriptional signature of human microglia: derivation and utility in describing region-dependent alterations associated with Alzheimer's disease. *Glia*. 2019;67:1240-1253. https://doi.org/10.1002/glia.23572. Epub 2019/02/14. PubMed PMID: 30758077.
59. Morimoto K, Nakajima K. Role of the immune system in the development of the central nervous system. *Front Neurosci*. 2019;13:916. https://doi.org/10.3389/fnins.2019.00916. Epub 2019/09/26. PubMed PMID: 31551681; PMCID: PMC6735264.
60. Tovar YRLB, Kolson DL, Bandaru VV, Drewes JL, Graham DR, Haughey NJ. Adenosine triphosphate released from HIV-infected macrophages regulates glutamatergic tone and dendritic spine density on neurons. *J Neuroimmune Pharmacol*. 2013;8:998-1009. https://doi.org/10.1007/s11481-013-9471-7. Epub 2013/05/21. PubMed PMID: 23686368; PMCID: PMC3740066.
61. Cserep C, Posfai B, Lenart N, et al. Microglia monitor and protect neuronal function through specialized somatic purinergic junctions. *Science*. 2020;367:528-537. https://doi.org/10.1126/science.aax6752. Epub 2019/12/14. PubMed PMID: 31831638.
62. Deczkowska A, Weiner A, Amit I. The physiology, pathology, and potential therapeutic applications of the TREM2 signaling pathway. *Cell*. 2020;181:1207-1217. https://doi.org/10.1016/j.cell.2020.05.003. Epub 2020/06/13. PubMed PMID: 32531244.
63. Keren-Shaul H, Spinrad A, Weiner A, et al. A unique microglia type associated with restricting development of Alzheimer's disease. *Cell*. 2017;169:1276-90 e17. https://doi.org/10.1016/j.cell.2017.05.018. Epub 2017/06/13. PubMed PMID: 28602351.
64. Rangaraju S, Dammer EB, Raza SA, et al. Identification and therapeutic modulation of a pro-inflammatory subset of disease-associated-microglia in Alzheimer's disease. *Mol Neurodegener*. 2018;13:24.

https://doi.org/10.1186/s13024-018-0254-8. Epub 2018/05/23. PubMed PMID: 29784049; PMCID: PMC5963076.

65. Huang L, Fang X, Shi D, et al. MSP-RON pathway: potential regulator of inflammation and innate immunity. *Front Immunol*. 2020;11:569082. https://doi.org/10.3389/fimmu.2020.569082. Epub 2020/10/30. PubMed PMID: 33117355; PMCID: PMC7577085.
66. Platanias LC. Mechanisms of type-I- and type-II-interferon-mediated signalling. *Nat Rev Immunol*. 2005;5:375-386. https://doi.org/10.1038/nri1604. Epub 2005/05/03. PubMed PMID: 15864272.
67. Behrens EM, Koretzky GA. Review: cytokine storm syndrome: looking toward the precision medicine era. *Arthritis Rheumatol*. 2017;69:1135-1143. https://doi.org/10.1002/art.40071. Epub 2017/02/22. PubMed PMID: 28217930.
68. Roberts ES, Zandonatti MA, Watry DD, et al. Induction of pathogenic sets of genes in macrophages and neurons in NeuroAIDS. *Am J Pathol*. 2003;162:2041-2057. https://doi.org/10.1016/S0002-9440(10)64336-2. Epub 2003/05/22. PubMed PMID: 12759259; PMCID: PMC1868118.
69. Masliah E, Roberts ES, Langford D, et al. Patterns of gene dysregulation in the frontal cortex of patients with HIV encephalitis. *J Neuroimmunol*. 2004;157:163-175. https://doi.org/10.1016/j.jneuroim.2004.08.026. Epub 2004/12/08. PubMed PMID: 15579294.
70. Roberts ES, Masliah E, Fox HS. CD163 identifies a unique population of ramified microglia in HIV encephalitis (HIVE). *J Neuropathol Exp Neurol*. 2004;63:1255-1264. https://doi.org/10.1093/jnen/63.12.1255. Epub 2004/12/31. PubMed PMID: 15624762.
71. Burdo TH, Soulas C, Orzechowski K, et al. Increased monocyte turnover from bone marrow correlates with severity of SIV encephalitis and CD163 levels in plasma. *PLoS Pathog*. 2010;6:e1000842. https://doi.org/10.1371/journal.ppat.1000842. Epub 2010/04/27. PubMed PMID: 20419144; PMCID: PMC2855320.
72. Burdo TH, Lentz MR, Autissier P, et al. Soluble CD163 made by monocyte/macrophages is a novel marker of HIV activity in early and chronic infection prior to and after anti-retroviral therapy. *J Infect Dis*. 2011;204:154-163. https://doi.org/10.1093/infdis/jir214. Epub 2011/06/02. PubMed PMID: 21628670; PMCID: PMC3105035.
73. Burdo TH, Weiffenbach A, Woods SP, Letendre S, Ellis RJ, Williams KC. Elevated sCD163 in plasma but not cerebrospinal fluid is a marker of neurocognitive impairment in HIV infection. *AIDS*. 2013;27:1387-1395. https://doi.org/10.1097/QAD.0b013e32836010bd. Epub 2013/02/26. PubMed PMID: 23435298; PMCID: PMC3844286.
74. Bryant AK, Moore DJ, Burdo TH, et al. Plasma soluble CD163 is associated with postmortem brain pathology in human immunodeficiency virus infection. *AIDS*. 2017;31:973-979. https://doi.org/10.1097/QAD.0000000000001425. Epub 2017/03/01. PubMed PMID: 28244955; PMCID: PMC5373961.
75. Burdo TH, Ellis RJ, Fox HS. Osteopontin is increased in HIV-associated dementia. *J Infect Dis*. 2008;198:715-722. https://doi.org/10.1086/590504. Epub 2008/07/12. PubMed PMID: 18616394; PMCID: PMC2587027.
76. Brown A, Islam T, Adams R, et al. Osteopontin enhances HIV replication and is increased in the brain and cerebrospinal fluid of HIV-infected individuals. *J Neurovirol*. 2011;17:382-392. https://doi.org/10.1007/s13365-011-0035-4. Epub 2011/05/11. PubMed PMID: 21556958; PMCID: PMC3331788.

SUPPORTING INFORMATION

Additional supporting information can be found online in the Supporting Information section at the end of this article.

How to cite this article: Trease AJ, Niu M, Morsey B, et al. Antiretroviral therapy restores the homeostatic state of microglia in SIV-infected rhesus macaques. *J Leukoc Biol*. 2022;112:969–981.
https://doi.org/10.1002/JLB.3HI0422-635R